Check for updates

High Power Laser Science and Engineering, (2026), Vol. 14, e14, 9 pages.
doi:10.1017/hpl.2026.10121

HIGH POWER LASER SCIENCE AND ENGINEERING

RESEARCH ARTICLE

Generation of polarization-tunable hybrid cylindrical vector γ rays from rotating electron beams

Si-Man Liu[1,†], Yue Cao[1,†], Kun Xue[2], Li-Xiang Hu[1], Xin-Yu Liu[1], Xin-Yan Li[1], Chao-Zhi Li[1], Xin-Rong Xu[1], Ke Liu[1], Wei-Quan Wang[1], De-Bin Zou[1], Yan Yin[1], Jian-Xing Li[2,3], and Tong-Pu Yu[1]

[1]*College of Science, National University of Defense Technology, Changsha, China*

[2]*Ministry of Education Key Laboratory for Nonequilibrium Synthesis and Modulation of Condensed Matter, State Key Laboratory of Electrical Insulation and Power Equipment, Shaanxi Province Key Laboratory of Quantum Information and Quantum Optoelectronic Devices, School of Physics, Xi'an Jiaotong University, Xi'an, China*

[3]*Department of Nuclear Physics, China Institute of Atomic Energy, Beijing, China*

(Received 5 December 2025; revised 18 January 2026; accepted 20 February 2026)

Abstract

Cylindrical vector (CV) γ rays can introduce spatially structured polarization as a new degree of freedom for fundamental research and practical applications. However, their generation and control remain largely unexplored. Here, we put forward a novel method to generate CV γ rays with tunable hybrid polarization via a rotating electron beam interacting with a solid foil. In this process, the beam generates a coherent transition radiation field and subsequently emits γ rays through nonlinear Compton scattering. By manipulating the initial azimuthal momentum of the beam, the polarization angle of γ rays relative to the transverse momentum can be controlled, yielding tunable hybrid CV polarization states. Three-dimensional spin-resolved particle-in-cell simulations demonstrate continuous tuning of the polarization angle across $(-90°, 90°)$ with a high polarization degree exceeding 60%. Our work contributes to the development of structured γ rays, potentially opening up new avenues in high-energy physics, nuclear science and laboratory astrophysics.

Keywords: coherent transition radiation; cylindrical vector γ rays; nonlinear Compton scattering; rotating electron beams

1. Introduction

The polarization of γ rays plays a crucial role in exploring diverse fields, including high-energy physics[1–4], nuclear physics[5–7], materials science[8,9] and laboratory astrophysics[10–12]. Specifically, circularly polarized γ rays serve as powerful probes of parity violation[13], elastic photon–photon scattering[14] and photoproduction of mesons[15]. Meanwhile, linearly polarized γ rays prove essential in nuclear resonance fluorescence imaging[16], probing linear Breit–Wheeler pair production[17,18] and exploring vacuum birefringence[3,4,19]. Beyond these homogeneous polarization states, beams with spatially varying polarization, as a class of structured beams, have attracted considerable attention in optics[20–22]. A particular class is the cylindrical vector (CV) beam[23,24], which includes beams with radial, azimuthal or hybrid polarization (a linear superposition of radial and azimuthal polarization). These distinct polarization states have enabled various applications, including high-resolution imaging and focusing with radially polarized beams[25–27], trapping and manipulation of particles with azimuthally polarized beams[28–32] and high-capacity optical communications with hybrid polarization states[33]. Extending CV polarization to the γ-ray regime would introduce spatial distribution of polarization as a new degree of freedom for γ-ray applications. Furthermore, the ability to actively control this polarization topology, for instance, by continuously tuning it from radial to azimuthal states, would further unlock unprecedented opportunities in broad fields, such as probing or manipulating nuclear and subnuclear structures[34–37], and investigating photon emission with radial and azimuthal polarization in laboratory astrophysics[38].

Despite the potential highlighted above, the tunable generation of such CV γ rays remains a significant challenge. In the optical domain, components such as spatial light modulators[39,40] and Q-plates[41,42] enable flexible polarization

Correspondence to: K. Xue, School of Physics, Xi'an Jiaotong University, Xi'an 710049, China. Email: xuekun@xjtu.edu.cn; T.-P. Yu, College of Science, National University of Defense Technology, Changsha 410073, China. Email: tongpu@nudt.edu.cn

[†]These authors contributed equally to this work.

© The Author(s), 2026. Published by Cambridge University Press in association with Chinese Laser Press. This is an Open Access article, distributed under the terms of the Creative Commons Attribution licence (https://creativecommons.org/licenses/by/4.0), which permits unrestricted re-use, distribution and reproduction, provided the original article is properly cited.

https://doi.org/10.1017/hpl.2026.10121 Published online by Cambridge University Press

manipulation of CV beams, transforming homogeneously polarized beams into CV beams with continuously tunable polarization. However, these optical components that rely on properties such as birefringence and dichroism are not readily applicable to γ rays, as the short wavelengths present challenges for their modulation capabilities[24,43].

On the other hand, existing schemes for producing and manipulating polarized γ rays primarily focus on circularly or linearly polarized γ rays, lacking the capability to generate spatially varying polarization states. For instance, in linear Compton scattering, the polarization of the driving laser can determine the circular or linear polarization of γ rays[44–51]. In incoherent bremsstrahlung, circularly polarized γ rays can be generated using longitudinally spin-polarized electrons interacting with metal targets[52–54], while linearly polarized γ rays require electron beam–crystal interactions through coherent bremsstrahlung[55–57]. The advent of high-intensity lasers has enabled γ-ray generation via the nonlinear Compton scattering process, yielding brilliant, high-energy polarized γ rays. In this nonlinear regime, the polarization of γ rays can be controlled through electron polarization and laser polarization, with longitudinally spin-polarized electrons generating circular polarization[58] and transversely polarized electrons[58] or laser polarization[59,60] producing linear polarization. However, the development of tunable sources of γ rays with spatially varying polarization has received limited attention. Recent works have shown that complex electron dynamics can imprint spatial structures onto the polarization of the γ-ray emission, offering powerful diagnostic tools for plasma interactions and inspiring the development of structured γ rays[61,62]. Our recent work[63] took an important step towards this goal by presenting a potential approach to generating CV γ rays. Yet, the continuous tuning of hybrid CV polarization states remains a significant challenge.

This challenge may be addressed by introducing a new property to the seed electron beam. Recent studies have shown that accelerating electrons with lasers carrying orbital angular momentum, such as Laguerre–Gaussian laser pulses[64,65], can produce electron beams with azimuthal momentum. Alternative approaches, such as multiple Gaussian laser pulses interacting with plasmas[66], or a Gaussian laser pulse interacting with a beam-splitting array[67], can also generate such rotating beams, improving experimental feasibility. These electron beams with significant azimuthal momentum offer numerous potential applications, including wakefield acceleration[68,69] and attosecond bunch generation[64]. However, the direct measurement of beam azimuthal momentum is difficult in experiments and has received limited attention[70].

In this paper, we put forward a novel scheme for the generation of polarization-tunable hybrid CV γ rays via the interaction of a rotating electron beam with a solid foil, where the polarization of the emitted photons can be tuned efficiently

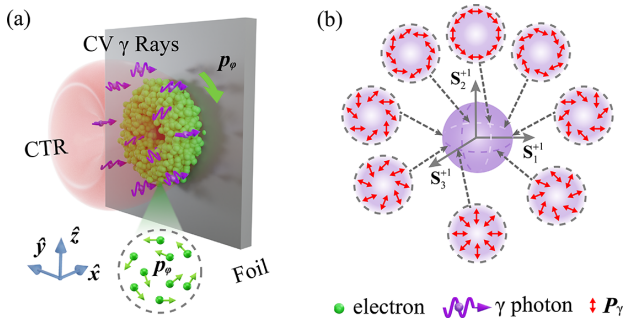


Figure 1. Schematic diagram for hybrid cylindrical vector (CV) γ-ray emission through the interaction of a rotating electron beam and a foil. (a) A relativistic electron beam carrying azimuthal momentum p_φ propagates in the $+x$ direction and traverses a foil, resulting in coherent transition radiation (CTR) and producing polarized γ rays through the nonlinear Compton scattering process. The green arrows indicate the azimuthal momentum p_φ of the beam. (b) Higher-order Poincaré sphere for topological charge $l = 1$, where all states on the surface are CV polarized. Points on the equator represent the hybrid mode polarized γ rays that can be generated in this scheme. Here, $\mathbf{S}_3^{+1} = \pm 1$ represents radial and azimuthal polarizations, respectively, while $\mathbf{S}_1^{+1} = \pm 1$ corresponds to polarization directions at 45° and 135° with respect to the radial direction, respectively.

by the initial azimuthal momentum of the beam. As shown in Figure 1(a), when the seed electron beam carrying azimuthal momentum interacts with the foil, it generates a coherent transition radiation (CTR) field, which in turn leads to photon emission through the nonlinear Compton scattering process. Manipulating the initial azimuthal momentum of the electrons can control the angle between the polarization direction and transverse momentum of the emitted photons, thereby resulting in tunable hybrid CV polarization states, as shown in Figure 1(b). Moreover, the relationship between the electron azimuthal momentum and γ-ray polarization state could also serve as a potential tool for detecting electron azimuthal momentum in the laboratory. Three-dimensional spin-resolved quantum electrodynamics (QED) particle-in-cell (PIC) simulations demonstrate the generation of high-energy γ rays with a high polarization degree exceeding 60%. Our work contributes to the active manipulation of the polarization topology of γ rays, and could offer a promising tool for investigations in diverse areas, such as high-energy physics[19], nuclear science[34–37] and laboratory astrophysics[38].

2. Simulation methods and setup

We perform simulations using the spin-resolved QED PIC code SLIPs[71], which is coupled to a Monte Carlo algorithm for QED processes based on the local constant field approximation[45,72–74]. As one of the primary QED processes during the beam–target interaction, the nonlinear Compton scattering process is characterized by the nonlinear QED parameter $\chi_e \equiv |e|\hbar/\left(m_e^3c^4\right)\sqrt{-\left(F_{\mu\nu}p^\nu\right)^2}$[75–77]. Here,

https://doi.org/10.1017/hpl.2026.10121 Published online by Cambridge University Press

e and m_e are the charge and mass of the electron, respectively, c is the speed of light in vacuum, $\hbar$ is the reduced Planck constant, p^ν is the four-momentum of the electron and $F_{\mu\nu}$ is the electromagnetic field tensor. In nonlinear Compton scattering, the polarization of a γ photon can be described by the Stokes parameters (ξ_1, ξ_2, ξ_3). Since the polarization of an emitted γ photon is associated with the directions of the velocity $\widehat{\mathbf{v}}$ and acceleration $\widehat{\mathbf{a}}$ of the parent electron, we define the polarization in an instantaneous frame $(\widehat{\mathbf{k}}_\gamma, \widehat{\mathbf{e}}_1, \widehat{\mathbf{e}}_2)$[78] comoving with the electron, with $\widehat{\mathbf{e}}_1 = \widehat{\mathbf{a}} - \widehat{\mathbf{v}}(\widehat{\mathbf{v}}\cdot\widehat{\mathbf{a}})$ and $\widehat{\mathbf{e}}_2 = \widehat{\mathbf{v}} \times \widehat{\mathbf{a}}$. Here, the direction of photon propagation $\widehat{\mathbf{k}}_\gamma$ is considered to be aligned with $\widehat{\mathbf{v}}$, since the emission angle is approximately $1/\gamma_e \ll 1$, where γ_e is the Lorentz factor of the electron. On this basis, ξ_3 corresponds to the degree of linear polarization along $\widehat{\mathbf{e}}_1$ versus $\widehat{\mathbf{e}}_2$; ξ_1 represents linear polarization at an angle of $\pm 45°$ to the $\widehat{\mathbf{e}}_1$-axis; and ξ_2 denotes the degree of circular polarization[79]. This instantaneous frame changes as the electron moves. To detect the mean polarization of photons propagating in a given direction, their Stokes parameters must be transformed to a common observation frame $(\widehat{\mathbf{k}}_\gamma, \widehat{\mathbf{o}}_1, \widehat{\mathbf{o}}_2)$ and then averaged.

The average Stokes parameters of a photon emitted by an electron with initial spin $\mathbf{S}_i$ are given by the following[63]:

$$\overline{\xi}_1 = \frac{u/(1-u)\, K_{\frac{1}{3}}(\rho)\,(\mathbf{S}_i \cdot \widehat{\mathbf{a}})}{w - uK_{\frac{1}{3}}(\rho)\,\widehat{\mathbf{b}}\cdot\mathbf{S}_i}, \tag{1a}$$

$$\overline{\xi}_2 = \frac{-\left[u\mathrm{Int}K_{\frac{1}{3}}(\rho) - \left(2u-u^2\right)/(1-u)\, K_{\frac{2}{3}}(\rho)\right](\mathbf{S}_i \cdot \widehat{\mathbf{v}})}{w - uK_{\frac{1}{3}}(\rho)\,\widehat{\mathbf{b}}\cdot\mathbf{S}_i}, \tag{1b}$$

$$\overline{\xi}_3 = \frac{K_{\frac{2}{3}}(\rho) - u(1-u)\, K_{\frac{1}{3}}(\rho)\left(\mathbf{S}_i \cdot \widehat{\mathbf{b}}\right)}{w - uK_{\frac{1}{3}}(\rho)\,\widehat{\mathbf{b}}\cdot\mathbf{S}_i}, \tag{1c}$$

where $w = -\mathrm{Int}K_{\frac{1}{3}}(\rho) + \frac{u^2-2u+2}{1-u}K_{\frac{2}{3}}(\rho)$, $\widehat{\mathbf{b}} = \widehat{\mathbf{v}} \times \widehat{\mathbf{a}}/|\widehat{\mathbf{v}} \times \widehat{\mathbf{a}}|$, $\rho = 2u/[(1-u)3\chi_e]$, $u = \omega_\gamma/\varepsilon_i$ is the ratio of the photon energy ω_γ to the initial electron energy ε_i, and $\mathrm{Int}K_{\frac{1}{3}}(\rho) \equiv \int_\rho^\infty \mathrm{d}z K_{\frac{1}{3}}(z)$, with K_n being the nth-order modified Bessel function of the second kind. The degree of polarization for each propagation direction $\widehat{\mathbf{k}}_\gamma$ is given by $P_\gamma \equiv \sqrt{\overline{\xi_1}^2 + \overline{\xi_3}^2}$.

The simulation box has dimensions of $x \times y \times z = 7\,\mu\mathrm{m} \times 10\,\mu\mathrm{m} \times 10\,\mu\mathrm{m}$, with grid cells of $560 \times 400 \times 400$. A rotating electron beam with an energy of 1 GeV, a charge of 1.73 nC, a relative energy spread of 5% and an angle spread of 0.5° propagates along the $+x$-axis. Here, the 'rotation' refers to electrons possessing an initial azimuthal momentum that leads to helical trajectories. This is distinct from electrons in a quantum vortex state[80]. Given that an electron beam with azimuthal momentum possesses a hollow density profile as a result of centrifugal forces, we specify the initial beam density in our simulations as $n_b = n_{b0}\exp\left[-x^2/\sigma_x^2 - (r-r_c)^2/\sigma_\perp^2\right]$. Here, $r = \sqrt{y^2+z^2}$, $\sigma_x = 0.5\ \mu\mathrm{m}$, $r_c = \sigma_\perp = 1\ \mu\mathrm{m}$ and n_{b0} is the maximum density of the beam. Here, $n_{b0} = 1.1 \times 10^{21}\ \mathrm{cm}^{-3}$ has been employed to generate a strong enough CTR field for nonlinear Compton scattering. This density must remain below the foil density to prevent target penetration, which would suppress the CTR field[81]. Electron beams with comparable parameters can be produced using advanced conventional accelerators or laser-driven accelerators[82–86], as detailed in the Supplementary Material. A solid aluminum foil with density $n_{Al} = 5.4 \times 10^{22}\ \mathrm{cm}^{-3}$ and thickness $d = 0.5\ \mu\mathrm{m}$ is employed with its front surface at $x = 5\ \mu\mathrm{m}$. In this scheme, thin, low-Z targets are preferred to suppress unwanted energy loss via bremsstrahlung and Bethe–Heitler processes, since both cross-sections scale approximately as Z^2[87]. In our setup, the contributions of these processes are simulated using the EPOCH code[88], as detailed in the Supplementary Material. A moving window is used, starting at $t = 8.25$ fs and moving along the $+x$-axis at a speed of c. In the simulations, each cell contains 10 macroparticles for beam electrons and aluminum atoms. In addition, field ionization is modeled using a hybrid approach that incorporates both tunnel ionization[89] and barrier-suppression ionization[90].

3. Generation and properties of hybrid cylindrical vector γ rays

The main results for the generated γ rays are summarized in Figure 2, which compares three cases with different initial azimuthal momenta of the electron: $p_\varphi = 10m_ec$ (Figures 2(a1) and 2(b1)), $20m_ec$ (Figures 2(a2) and 2(b2)) and $40m_ec$ (Figures 2(a3) and 2(b3)). Here, only photons with energies above 1 MeV are analyzed to focus on the high-energy γ rays. As shown in Figure 2(a), the emitted γ rays exhibit hybrid CV polarization. With increasing $|p_\varphi|$, the radial polarization component gradually decreases, whereas the azimuthal polarization component gradually increases. Since the angle-resolved distribution and polarization degree of the emitted γ rays exhibit cylindrical symmetry, we analyze their dependence on the polar angle θ, as shown in Figure 2(b). As $|p_\varphi|$ increases, the polar angle θ at the peak of γ-ray number rises approximately linearly with $|p_\varphi|$, reaching 0.3°, 0.6° and 1.2° for $p_\varphi = 10m_ec$, $20m_ec$ and $40m_ec$, respectively. In all cases, most of the γ rays distribute within a θ width of 0.8°. Furthermore, the degree of polarization increases with $|p_\varphi|$, with average polarization degrees of 0.44, 0.57 and 0.65 for the cases shown in Figures 2(b1), 2(b2) and 2(b3), respectively. This enhancement occurs because a larger p_φ more effectively suppresses the polarization cancellation, which will be discussed in detail in Figure 3. The result of average polarization degrees is comparable to that achieved in laser–electron collision schemes (~60%)[58,60].

https://doi.org/10.1017/hpl.2026.10121 Published online by Cambridge University Press

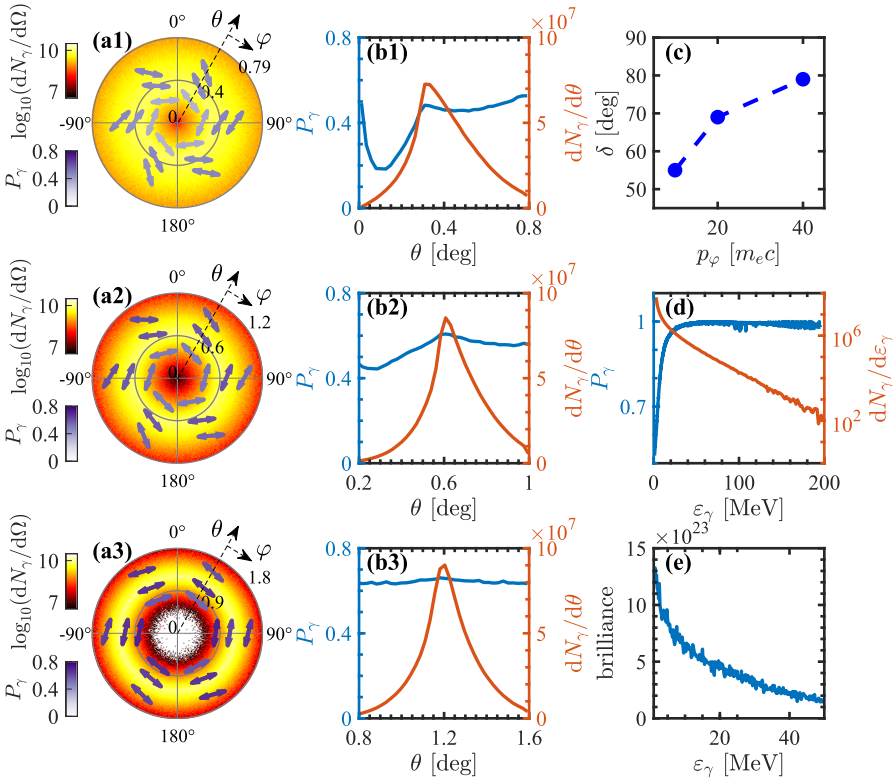


Figure 2. (a1)–(a3) Angle-resolved distribution $\log_{10}\left(\mathrm{d}N_\gamma/\mathrm{d}\Omega\right)$ (background heatmap) and average polarization P_γ of the emitted γ photons with respect to the polar angle θ and the azimuth angle φ. Here, $\mathrm{d}\Omega = \sin\theta \mathrm{d}\theta\mathrm{d}\varphi$, where θ is the angle between the photon momentum and the $+x$-axis, and φ is the angle between the projection of the momentum onto the yz-plane and the $+y$-axis. The superimposed double-headed arrows indicate the average polarization direction, while their color represents the degree of polarization P_γ. (b1)–(b3) Angle-resolved polarization degree P_γ (blue) and distribution $\mathrm{d}N_\gamma/\mathrm{d}\theta$ (red) of all emitted γ photons versus θ. Here, panels ((a1), (b1)), ((a2), (b2)) and ((a3), (b3)) correspond to the case with an initial electron azimuthal momentum of $p_\varphi = 10m_\mathrm{e}c$, $20m_\mathrm{e}c$ and $40m_\mathrm{e}c$, respectively. (c) The angle δ as a function of the electron initial azimuthal momentum p_φ. (d) Energy-resolved polarization degree P_γ (blue) and distribution $\mathrm{d}N_\gamma/\mathrm{d}\varepsilon_\gamma$ (red) of γ photons within $0.15° < \theta < 0.65°$ versus the photon energy ε_γ for $p_\varphi = 20m_\mathrm{e}c$. (e) The brilliance (photons/$\left(\mathrm{s\ mm^2\ mrad^2} \times 0.1\%\ \mathrm{bandwidth}\right)$) of the γ rays as a function of the photon energy ε_γ.

The hybrid CV polarization state is characterized by a polarization angle δ, defined as the angle between the polarization direction $\widehat{\mathbf{e}}_\mathrm{P}$ and the radial unit vector $\widehat{\mathbf{e}}_\mathrm{r}$. Here, $\delta = 0°$ corresponds to purely radial polarization, while $|\,\delta\,| = 90°$ corresponds to purely azimuthal polarization. Our simulations show that $|\,\delta\,|$ increases with $|\,p_\varphi\,|$, reaching 55°, 69° and 79° at $p_\varphi = 10m_\mathrm{e}c$, $20m_\mathrm{e}c$ and $40m_\mathrm{e}c$, respectively (Figure 2(c)), with a limit of 90°. This dependence makes it possible to diagnose the azimuthal momentum of short-pulse electron beams, which remains a great challenge in current laboratories[70]. Since the sign of δ is determined by the sign of p_φ, the angle δ can cover the range $(-90°, 90°)$.

We now discuss the energy dependence of the γ-ray properties, using the case of $p_\varphi = 20m_\mathrm{e}c$ as an example. Figure 2(d) shows the energy-resolved polarization P_γ and energy spectrum $\mathrm{d}N_\gamma/\mathrm{d}\varepsilon_\gamma$ of photons within $0.15° < \theta < 0.65°$ for the case of $p_\varphi = 20m_\mathrm{e}c$. These γ rays exhibit an exponential energy spectrum with a cutoff at approximately 200 MeV. The average polarization increases with photon energy ε_γ from approximately 60% at the MeV range to nearly 100% above 25 MeV. This trend is consistent with the theoretical prediction, as shown in Figure 3(c), that P_γ increases with $\varepsilon_\gamma/\varepsilon_\mathrm{e}$ over our parameter range ($\varepsilon_\gamma/\varepsilon_\mathrm{e} < 0.2, \varepsilon_\mathrm{e} \sim 1$ GeV). These photons have a root-mean-square angular divergence of 0.79 mrad× 0.79 mrad, and spatial dimensions of 0.22 μm (longitudinal) and 1.20 μm × 1.20 μm (transverse). The corresponding brilliances at $\varepsilon_\gamma = 1$, 10 and 50 MeV are 1.37×10^{24}, 7.86×10^{23} and 1.43×10^{23} photons/$\left(\mathrm{s\ mm^2\ mrad^2} \times 0.1\%\ \mathrm{bandwidth}\right)$, respectively, as shown in Figure 2(e).

4. Mechanism of γ-ray polarization

When a relativistic electron beam traverses a target, the abrupt change in dielectric constant generates an intense CTR field on both sides of the target[91,92], as shown in Figure 3(a). This leads to substantial γ-ray emission from the beam electrons via the nonlinear Compton scattering process. In a cylindrical coordinate system aligned with the x-axis $(\widehat{\mathbf{e}}_x, \widehat{\mathbf{e}}_\mathrm{r}, \widehat{\mathbf{e}}_\vartheta)$, this field takes the form $\mathbf{E}_\mathrm{CTR} = E_\mathrm{r}\widehat{\mathbf{e}}_\mathrm{r} + E_x\widehat{\mathbf{e}}_x$ and $\mathbf{B}_\mathrm{CTR} = -B_\vartheta\widehat{\mathbf{e}}_\vartheta$[81]. For relativistic electrons propagating along the x-axis, the effective electric field can be written as $\mathbf{E}' = \mathbf{E}_\perp + \mathbf{v}\times\mathbf{B} \approx (E_\mathrm{r} + cB_\vartheta)\widehat{\mathbf{e}}_\mathrm{r}$, where $\mathbf{E}_\perp$ is the transverse

https://doi.org/10.1017/hpl.2026.10121 Published online by Cambridge University Press

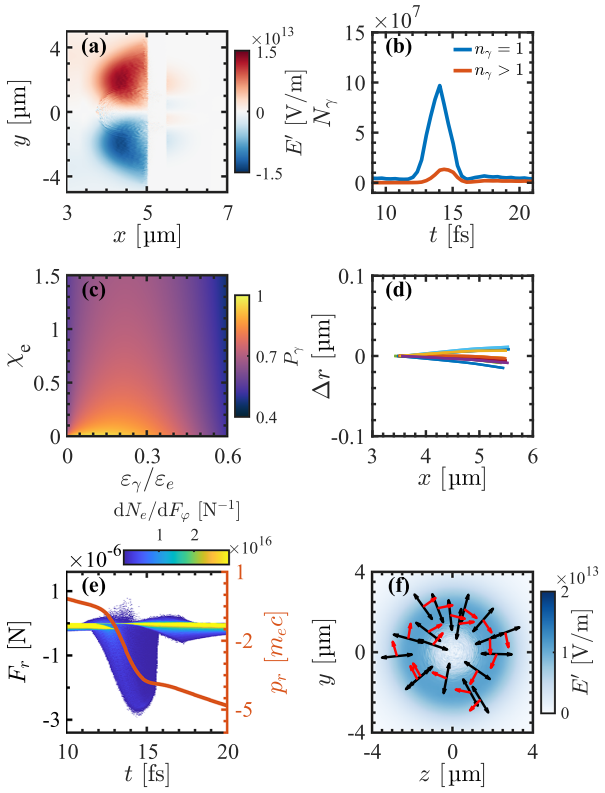


Figure 3. (a) Distribution of the effective electric field E' in the xy-plane at $z = 0$. (b) Time-dependent photon generation rate, where the blue line represents the rate for first-photon emission and the red line represents the rate for multiple-photon emission. (c) Average polarization degree P_γ as a function of energy ratio $\varepsilon_\gamma/\varepsilon_e$ and QED parameter χ_e. (d) Radial displacement as a function of longitudinal position for selected electrons during interaction with the CTR field. (e) Distribution of radial forces F_r acting on electrons at different times, with color representing the number of electrons. The red solid line shows the evolution of the average radial momentum p_r of the beam. (f) Distribution of photon polarization directions (black double arrows) and momentum directions (red arrows) in the yz-plane, with the color scale representing the effective electric field E'.

electric field. The intensity of the γ-ray emission is governed by the nonlinear QED parameter $\chi_e \approx \gamma_e \mid \mathbf{E}' \mid /E_c$[45], where $E_c = m_e^2 c^3/(|e|\hbar) \approx 1.3 \times 10^{18}$ V/m is the Schwinger critical field. The CTR field comprises components propagating along both the $-x$ and $+x$ directions. Electrons interacting with the field propagating along $-x$ experience a large χ_e, thereby dominating the γ-ray emission, while the contribution from the field propagating along $+x$ is negligible.

As depicted in Figure 3(b), high-energy photons primarily originate from single photon emissions from electrons, with multiple photon emissions accounting for only about 5.5% of the total photons. This is due to the significant reduction in electron energy and the corresponding decrease in χ_e after the first emission. Consequently, we consider only the first photon emitted by an electron. For an initially unpolarized electron beam, the initial spin averages to zero ($\overline{\mathbf{S}_i} = 0$). This leads to a simplification of Equation (1), yielding $\overline{\xi_1} = \overline{\xi_2} = 0$ and a non-zero $\overline{\xi_3} = K_{\frac{2}{3}}(\rho)/w$. This result indicates that the emitted photon is linearly polarized along the axis $\hat{\mathbf{e}}_1$ of the instantaneous frame. In this case, the degree of polarization is given by $P_\gamma = \overline{\xi_3} = (1-u)K_{2/3}(\rho)/\left[-(1-u)\mathrm{Int}K_{1/3}(\rho) + \left(u^2-2u+2\right)\cdot K_{2/3}(\rho)\right]$. As illustrated in Figure 3(c), P_γ decreases with increasing χ_e at a fixed ε_γ; conversely, at a fixed χ_e, P_γ first increases with the photon energy ε_γ, reaches a maximum, and then decreases to zero. In our scheme, since the emitted γ photons have small polar angles and electrons exhibit negligible radial displacement [Figure 3(d)], we can approximate the velocity of the parent electron as $\hat{\mathbf{v}} \approx \hat{\mathbf{e}}_x$ and its transverse acceleration as $\hat{\mathbf{a}}_\perp \approx \mathbf{E}'/\mid \mathbf{E}' \mid \approx -\hat{\mathbf{e}}_r$. The $\hat{\mathbf{e}}_1$-axis of the instantaneous frame becomes $\hat{\mathbf{e}}_1^0 = \hat{\mathbf{a}} - \hat{\mathbf{v}}(\hat{\mathbf{v}}\cdot\hat{\mathbf{a}}) \approx -\hat{\mathbf{e}}_r \parallel -\mathbf{E}'$, which shows that the emitted γ photon is polarized along the radial direction. The remaining axes of the instantaneous frame are $\hat{\mathbf{k}}_\gamma \approx \hat{\mathbf{v}}$ and $\hat{\mathbf{e}}_2^0 = \hat{\mathbf{v}} \times \hat{\mathbf{a}} \approx -\hat{\mathbf{e}}_\vartheta$. As all photons with a given wavevector $\hat{\mathbf{k}}_\gamma$ share this common instantaneous frame ($\hat{\mathbf{k}}_\gamma$, $\hat{\mathbf{e}}_1^0$, $\hat{\mathbf{e}}_2^0$), we adopt it as our observation frame ($\hat{\mathbf{k}}_\gamma$, $\hat{\mathbf{o}}_1$, $\hat{\mathbf{o}}_2$).

The hybrid γ-ray polarization originates from the misalignment between their transverse momentum and polarization directions. During the interaction with the CTR field, an electron experiences a radial Lorentz force $\mathbf{F}_r$, and acquires a radial momentum component ($\sim 5 m_e c$ in Figure 3(e)). The azimuthal and radial momentum components of the parent electron (p_φ and p_r) are subsequently transferred to the emitted photon. Therefore, the direction of the photon transverse wave vector $\mathbf{k}_\perp$ deviates from the radial direction by an angle $\arctan\left(p_\varphi/p_r\right)$ (Figure 3(f)). As a result, for a given observation angle ϕ, the detected photons originate from electrons at a specific position $\vartheta = \phi - \arctan\left(p_\varphi/p_r\right)$, and their observed polarization is oriented at an angle $-\arctan\left(p_\varphi/p_r\right)$ relative to $\hat{\mathbf{e}}_r(\phi)$. Consequently, the polarization angle δ can be approximated as $\delta \approx \arctan\left(p_\varphi/p_r\right)$. By varying the initial azimuthal momentum p_φ, δ can be continuously tuned, yielding the different polarization states shown in Figure 2(a). Furthermore, since the intensity of the CTR field is proportional to the density of the driving electron beam[81], adjusting the beam density changes $\mathbf{F}_r$ and p_r, thereby providing an additional choice for manipulating the polarization states.

5. Influence of parameters

To demonstrate experimental feasibility, the impact of key parameters of the electron beam and the foil on the γ-ray polarization degree P_γ, number of the emitted photons N_γ and cutoff energy ε_m is summarized in Figure 4. Here, only one parameter is changed in each case, while all other parameters are kept fixed. As the electron azimuthal momentum p_φ increases, the polarization angle δ increases from approximately –90° to 90° (Figure 4(a)). This arises from the increase in $\arctan\left(p_\varphi/p_r\right)$, as the radial momentum p_r remains nearly constant. The scaling relationship between

https://doi.org/10.1017/hpl.2026.10121 Published online by Cambridge University Press

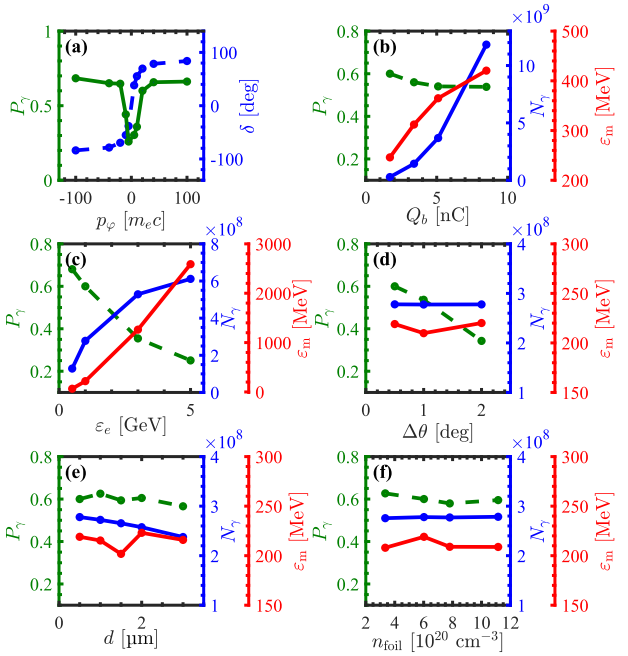


Figure 4. (a) Average polarization degree P_γ (green line) and polarization angle δ (blue line) as a function of azimuthal momentum p_φ. Effects of (b) charge of the electron beam Q_b, (c) energy of the electron beam ε_e, (d) beam angle spread $\Delta\theta$, (e) thickness of the foil and (f) density of the foil on the average polarization degree P_γ (green line), number of the emitted photons N_γ (blue line) and cutoff energy ε_m (red line).

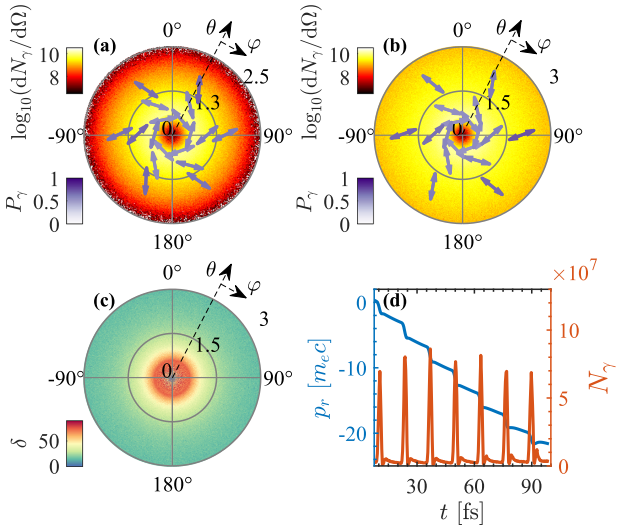


Figure 5. (a), (b) Angle-resolved distribution $\log_{10}(dN_\gamma/d\Omega)$ (background heatmap) and average polarization P_γ of the emitted γ rays, where (a) corresponds to electrons traversing three foils and (b) corresponds to seven foils. (c) Angle-resolved distribution of the γ-ray polarization angle δ, after traversing seven foils. (d) Evolution of the average radial momentum of electrons (blue line) and the number of radiated photons (red line).

p_φ and δ provides a potential method for diagnosing electron azimuthal momentum through γ-ray polarization state in the laboratory. Experimentally, detection of the polarization of CV γ rays would involve using a multi-aperture collimator to sample the γ rays into several beamlets at different azimuthal positions, and then measuring the local polarization of each beamlet with established techniques such as Compton polarimetry[93–95]. The CV polarization structure can thus be reconstructed from such measurements (see Supplementary Material for details). The average polarization degree P_γ rises with $|p_\varphi|$ and reaches 70%, since a larger $|p_\varphi|$ suppresses the polarization cancellation[63]. A higher electron charge Q_b strengthens the CTR field intensity, leading to an enhancement of $\mathbf{E}' \propto Q_b$. This subsequently increases $\chi_e \approx \gamma_e |\mathbf{E}'|/E_c$ and the radiation probability[58,60]. As shown in Figure 4(b), increasing Q_b leads to an increase in both the cutoff energy $\varepsilon_m \propto \chi_e \gamma_e$ and the number of radiated photons N_γ, while P_γ decreases (as discussed in Section 4). Similarly, increasing electron beam energy ε_e also increases χ_e, leading to consequently increasing N_γ and ε_m while decreasing P_γ, as illustrated in Figure 4(c). Conversely, an increase in the angle spread $\Delta\theta$ broadens the electron transverse momentum distribution, enhancing the polarization cancellation[63]. This leads to a reduction in the polarization degree, whereas the cutoff energy ε_m and the total photon yield N_γ remain stable, as shown in Figure 4(d).

The influence of foil parameters is also investigated. As the foil thickness d increases, the number of emitted photons N_γ decreases slightly, while both the polarization degree P_γ and cutoff energy ε_m remain almost unchanged, as shown in Figure 4(e). They spend more time traversing a thicker foil, thereby reducing the time for interacting with the CTR field propagating along the $+x$ direction and resulting in fewer γ-ray emissions at the same time. In contrast, the density of the target has a negligible impact on N_γ, P_γ and ε_m, according to Figure 4(f), since it has little influence on the CTR field[81].

We further investigate the interaction of the rotating electron beam with multiple foils. The results reveal a more complex polarization structure that can be controlled efficiently by varying the number of foils. For example, we use the electron beam with $p_\varphi = 20 m_e c$ and the foil separation of 4 μm. Here, all other parameters are identical to those in Section 3. As shown in Figures 5(a) and 5(b), the radial polarization component of the emitted γ rays increases with the polar angle θ for a given azimuthal angle φ. This θ-dependent polarization structure becomes clearer upon increasing the foil number, owing to the broader angular distribution of the emitted γ rays. For both $N_{foil} = 3$ (Figure 5(a)) and $N_{foil} = 7$ (Figure 5(b)), the polarization degree P_γ remains above 50%. (Figure 5(c)) displays the angular distribution of polarization angle of γ rays for $N_{foil} = 7$. The results reveal a clear decrease of δ from nearly 90° to approximately 10° with increasing polar angle θ. Specifically, the polarization is predominantly azimuthal at small θ, whereas it changes to predominantly radial at large θ.

Figure 5(d) reveals the origin of this polarization structure. Upon interacting with each foil, electrons gain radial

https://doi.org/10.1017/hpl.2026.10121 Published online by Cambridge University Press

momentum and emit γ rays through the CTR fields generated at each foil. As p_r accumulates with increasing the foil number, p_φ/p_r gradually decreases. At $N_{foil} = 7$, p_r eventually exceeds p_φ. This leads to a corresponding reduction in the polarization angle δ and an increase in the polar angle of the emitted γ rays. Consequently, γ rays generated at lower N_{foil} exhibit larger δ and concentrate around $\theta = 0°$ in the angular distribution, while those generated at higher N_{foil} have smaller δ and appear at larger θ. This gives rise to the polarization structure observed in Figures 5(a) and 5(b). The results demonstrate that the polarization is tunable by simply changing the foil number, thereby making it feasible in experiments.

6. Conclusion

In conclusion, we have put forward a novel method for generating polarization-tunable hybrid CV γ rays through the interaction of rotating electron beams with solid foils. Our approach achieves continuous tuning of the polarization angle δ across the range of $(-90°, 90°)$ by adjusting the beam azimuthal momentum p_φ. We establish a connection between p_φ and the polarization structure of the emitted γ rays, making it a potential probe for detecting the azimuthal momentum of driving electrons. Our work could offer a promising method for applications of structured γ rays in diverse areas, such as high-energy physics, nuclear science and laboratory astrophysics.

Acknowledgements

This work is supported by the National Natural Science Foundation of China (Grant Nos. 12135009, 12375244, 12175310 and 12505235), the Natural Science Foundation of Hunan Province of China (Grant No. 2025JJ30002), the China Postdoctoral Science Foundation (Grant No. 2024M762568), the Postdoctoral Fellowship Program of CPSF (Grant No. GZC20252248) and the Fundamental Research Funds for the Central Universities of Ministry of Education of China (Grant No. xzy012025079).

Supplementary material

The supplementary material for this article can be found at http://doi.org/10.1017/hpl.2026.10121.

References

1. G. Moortgat-Pick, T. Abe, G. Alexander, B. Ananthanarayan, A. A. Babich, V. Bharadwaj, D. Barber, A. Bartl, A. Brachmann, S. Chen, *et al.*, Phys. Rep. **460**, 131 (2008).
2. T. T. Qin, W. Luo, H. Y. Lan, and W. M. Wang, Matter Radiat. Extremes **7**, 035901 (2022).
3. S. Bragin, S. Meuren, C. H. Keitel, and A. Di Piazza, Phys. Rev. Lett. **119**, 250403 (2017).
4. C. Lv, F. Wan, Y. I. Salamin, Q. Zhao, M. Ababekri, R. R. Xu, and J. X. Li, Adv. Sci. **12**, e17201 (2025).
5. U. I. Uggerhøj, Rev. Mod. Phys. **77**, 1131 (2005).
6. J. M. Mueller, M. W. Ahmed, and H. R. Weller, Nucl. Instrum. Methods Phys. Res. A **754**, 57 (2014).
7. L. W. Fagg and S. S. Hanna, Rev. Mod. Phys. **31**, 711 (1959).
8. K. Vetter, R. Barnowksi, A. Haefner, T. H. Y. Joshi, R. Pavlovsky, and B. J. Quiter, Nucl. Instrum. Methods Phys. Res. A **878**, 159 (2018).
9. K. Shimazoe, M. Uenomachi, and H. Takahashi, Commun. Phys. **5**, 24 (2022).
10. P. Laurent, J. Rodriguez, J. Wilms, M. C. Bel, K. Pottschmidt, and V. Grinberg, Science **332**, 438 (2011).
11. T. P. Yu, K. Liu, J. Zhao, X. L. Zhu, Y. Lu, Y. Cao, H. Zhang, F. Q. Shao, and Z. M. Sheng, Rev. Mod. Plasma Phys. **8**, 24 (2024).
12. C. Bœhm, C. Degrande, O. Mattelaer, and A. C. Vincent, J. Cosmol. Astropart. Phys. 2017, 043 (**2017**).
13. M. M. Arani and S. Bayegan, Eur. Phys. J. A **49**, 117 (2013).
14. D. Micieli, I. Drebot, A. Bacci, E. Milotti, V. Petrillo, M. R. Conti, A. R. Rossi, E. Tassi, and L. Serafini, Phys. Rev. Accel. Beams **19**, 093401 (2016).
15. Z. Akbar, P. Roy, S. Park, V. Crede, A. V. Anisovich, I. Denisenko, E. Klempt, V. A. Nikonov, A. V. Sarantsev, K. P. Adhikari, *et al.*, Phys. Rev. C **96**, 065209 (2017).
16. W. Bertozzi and R. J. Ledoux, Nucl. Instrum. Methods Phys. Res. B **241**, 820 (2005).
17. Q. Zhao, L. Tang, F. Wan, B. C. Liu, R. Y. Liu, R. Z. Yang, J. Q. Yu, X. G. Ren, Z. F. Xu, Y. T. Zhao, Y. S. Huang, and J. X. Li, Phys. Rev. D **105**, L071902 (2022).
18. Q. Zhao, Y. X. Wu, M. Ababekri, Z. P. Li, L. Tang, and J. X. Li, Phys. Rev. D **107**, 096013 (2023).
19. Y.-N. Dai, K. Z. Hatsagortsyan, C. H. Keitel, and Y.-Y. Chen, Phys. Rev. D **110**, 012008 (2024).
20. H. Rubinsztein-Dunlop, A. Forbes, M. V. Berry, M. R. Dennis, D. L. Andrews, M. Mansuripur, C. Denz, C. Alpmann, P. Banzer, T. Bauer, E. Karimi, L. Marrucci, M. Padgett, M. Ritsch-Marte, N. M. Litchinitser, N. P. Bigelow, C. Rosales-Guzmán, A. Belmonte, J. P. Torres, T. W. Neely, M. Baker, R. Gordon, A. B. Stilgoe, J. Romero, A. G. White, R. Fickler, A. E. Willner, G. Xie, B. McMorran, and A. M. Weiner, J. Opt. **19**, 013001 (2016).
21. A. Forbes, M. De Oliveira, and M. R. Dennis, Nat. Photonics **15**, 253 (2021).
22. M. Piccardo, M. O. Cernaianu, J. P. Palastro, A. Arefiev, C. Thaury, J. Vieira, D. H. Froula, and V. Malka, Optica **12**, 732 (2025).
23. Q. W. Zhan, Adv. Opt. Photon. **1**, 1 (2009).
24. J. Chen, C. H. Wan, and Q. W. Zhan, Sci. Bull. **63**, 54 (2018).
25. M. Liu, Y. Z. Lei, L. Yu, X. Fang, Y. Ma, L. X. Liu, J. J. Zheng, and P. Gao, Nano **11**, 3395 (2022).
26. Y. Kozawa, D. Matsunaga, and S. Sato, Optica **5**, 86 (2018).
27. R. Dorn, S. Quabis, and G. Leuchs, Phys. Rev. Lett. **91**, 233901 (2003).
28. Y. J. Yang, Y. X. Ren, M. Z. Chen, Y. Arita, and C. Rosales-Guzmán, Adv. Photonics **3**, 034001 (2021).
29. S. E. Skelton, M. Sergides, R. Saija, M. A. Iatì, O. M. Maragó, and P. H. Jones, Opt. Lett. **38**, 28 (2013).
30. L. Huang, H. L. Guo, J. F. Li, L. Ling, B. H. Feng, and Z. Y. Li, Opt. Lett. **37**, 1694 (2012).
31. M. G. Donato, S. Vasi, R. Sayed, P. H. Jones, F. Bonaccorso, A. C. Ferrari, P. G. Gucciardi, and O. M. Maragò, Opt. Lett. **37**, 3381 (2012).
32. H. Moradi, V. Shahabadi, E. Madadi, E. Karimi, and F. Hajizadeh, Opt. Express **27**, 7266 (2019).

https://doi.org/10.1017/hpl.2026.10121 Published online by Cambridge University Press

33. J. Liu, Z. Wu, Q. Zeng, B. Zhang, J. Chen, J. Xiao, H. Ye, Y. Chen, J. Liu, X. Zhou, D. Y. Fan, and S. Q. Chen, Commun. Phys. **8**, 409 (2025).
34. C. Iliadis and U. Friman-Gayer, Eur. Phys. J. A **57**, 190 (2021).
35. A. Zilges, D. L. Balabanski, J. Isaak, and N. Pietralla, Prog. Part. Nucl. Phys. **122**, 103903 (2022).
36. A. Thiel, A. V. Anisovich, D. Bayadilov, B. Bantes, R. Beck, Y. Beloglazov, M. Bichow, S. Böse, K.-T. Brinkmann, T. Challand, *et al.*, Phys. Rev. Lett. **109**, 102001 (2012).
37. M. Gottschall, A. V. Anisovich, B. Bantes, D. Bayadilov, R. Beck, M. Bichow, S. Böse, K.-T. Brinkmann, T. Challand, V. Crede, *et al.*, Phys. Rev. Lett. **112**, 012003 (2014).
38. D. A. Prokhorov, Y. J. Yang, R. Ferrazzoli, J. Vink, P. Slane, E. Costa, S. Silvestri, P. Zhou, N. Bucciantini, A. Di Marco, *et al.*, Astron. Astrophys. **692**, A59 (2024).
39. P. García-Martínez, D. Marco, J. L. Martínez-Fuentes, M. del Mar Sánchez-López, and I. Moreno, Opt. Lasers Eng. **125**, 105859 (2020).
40. D. Maluenda, I. Juvells, R. Martínez-Herrero, and A. Carnicer, Opt. Express **21**, 5432 (2013).
41. D. Naidoo, F. S. Roux, A. Dudley, I. Litvin, B. Piccirillo, L. Marrucci, and A. Forbes, Nat. Photonics **10**, 327 (2016).
42. M. M. Sánchez-López, J. A. Davis, N. Hashimoto, I. Moreno, E. Hurtado, K. Badham, A. Tanabe, and S. W. Delaney, Opt. Lett. **41**, 13 (2015).
43. F. F. Zhao, X. F. Jing, and M. Z. Yu, J. Appl. Phys. **137**, 050701 (2025).
44. V. N. Baier, V. M. Katkov, and V. S. Fadin, *Radiation of Relativistic Electrons* (Atomizdat, 1973).
45. V. I. Ritus, J. Sov. Laser Res. **6**, 497 (1985).
46. T. Omori, M. Fukuda, T. Hirose, Y. Kurihara, R. Kuroda, M. Nomura, A. Ohashi, T. Okugi, K. Sakaue, T. Saito, J. Urakawa, M. Washio, and I. Yamazaki, Phys. Rev. Lett. **96**, 114801 (2006).
47. G. Alexander, J. Barley, Y. Batygin, S. Berridge, V. Bharadwaj, G. Bower, W. Bugg, F.-J. Decker, R. Dollan, Y. Efremenko, V. Gharibyan, C. Hast, R. Iverson, H. Kolanoski, J. Kovermann, K. Laihem, T. Lohse, K. T. McDonald, A. A. Mikhailichenko, G. A. Moortgat-Pick, P. Pahl, R. Pitthan, R. Pöschl, E. Reinherz-Aronis, S. Riemann, A. Schälicke, K. P. Schüler, T. Schweizer, D. Scott, J. C. Sheppard, A. Stahl, Z. M. Szalata, D. Walz, and A. W. Weidemann, Phys. Rev. Lett. **100**, 210801 (2008).
48. V. Petrillo, A. Bacci, C. Curatolo, I. Drebot, A. Giribono, C. Maroli, A. R. Rossi, L. Serafini, P. Tomassini, C. Vaccarezza, and A. Variola, Phys. Rev. ST Accel. Beams **18**, 110701 (2015).
49. G. P. An, Y. L. Chi, Y. L. Dang, G. Y. Fu, B. Guo, Y. S. Huang, C. He, X. C. Kong, X. F. Lan, J. C. Li, F. L. Liu, J. S. Shi, X. J. Sun, Y. Wang, J. L. Wang, L. Wang, Y. Y. Wei, G. Wu, G. L. Xu, X. F. Xi, G. J. Yang, C. L. Zhang, Z. Zhang, Z. P. Zheng, X. D. Zhang, and S. P. Zhang, Matter Radiat. Extremes **3**, 219 (2018).
50. Y. Wang, M. Ababekri, F. Wan, J. X. Wen, W. Q. Wei, Z. P. Li, H. T. Kang, B. Zhang, Y. T. Zhao, W. M. Zhou, and J. X. Li, Phys. Plasmas **31**, 053105 (2024).
51. C. R. Howell, M. W. Ahmed, A. Afanasev, D. Alesini, J. R. M. Annand, A. Aprahamian, D. L. Balabanski, S. V. Benson, A. Bernstein, C. R. Brune, *et al.*, J. Phys. G **49**, 010502 (2021).
52. H. Olsen and L. C. Maximon, Phys. Rev. **114**, 887 (1959).
53. A. Giulietti, N. Bourgeois, T. Ceccotti, X. Davoine, S. Dobosz, P. D'Oliveira, M. Galimberti, J. Galy, A. Gamucci, D. Giulietti, L. A. Gizzi, D. J. Hamilton, E. Lefebvre, L. Labate, J. R. Marquès, P. Monot, H. Popescu, F. Rèau, G. Sarri, P. Tomassini, and P. Martin, Phys. Rev. Lett. **101**, 105002 (2008).
54. F. Albert and A. G. R. Thomas, Plasma Phys. Control. Fusion **58**, 103001 (2016).
55. E. A. Kuraev, Y. M. Bystritskiy, M. Shatnev, and E. Tomasi-Gustafsson, Phys. Rev. C **81**, 055208 (2010).
56. M. L. Ter-Mikaelian, *High-Energy Electromagnetic Processes in Condensed Media* (John Wiley & Sons, 1972).
57. D. Lohmann, J. Peise, J. Ahrens, I. Anthony, H.-J. Arends, R. Beck, R. Crawford, A. Hünger, K. H. Kaiser, J. D. Kellie, Ch. Klümper, P. Krahn, A. Kraus, U. Ludwig, M. Schumacher, O. Selke, M. Schmitz, M. Schneider, F. Wissmann, and S. Wolf, Nucl. Instrum. Methods Phys. Res. A **343**, 494 (1994).
58. Y. F. Li, R. Shaisultanov, Y. Y. Chen, F. Wan, K. Z. Hatsagortsyan, C. H. Keitel, and J. X. Li, Phys. Rev. Lett. **124**, 014801 (2020).
59. F. Wan, Y. Wang, R. T. Guo, Y. Y. Chen, R. Shaisultanov, Z. F. Xu, K. Z. Hatsagortsyan, C. H. Keitel, and J. X. Li, Phys. Rev. Res. **2**, 032049 (2020).
60. K. Xue, Z. K. Dou, F. Wan, T. P. Yu, W. M. Wang, J. R. Ren, Q. Zhao, Y. T. Zhao, Z. F. Xu, and J. X. Li, Matter Radiat. Extremes **5**, 054402 (2020).
61. Z. Gong, K. Z. Hatsagortsyan, and C. H. Keitel, Phys. Rev. Res. **4**, L022024 (2022).
62. L. J. Cui, K. J. Wei, C. Lv, F. Wan, Y. I. Salamin, L. F. Cao, and J. X. Li, Phys. Rev. A **111**, 023505 (2025).
63. Y. Cao, K. Xue, S. M. Liu, Z. P. Li, L. X. Hu, X. Y. Liu, Z. K. Dou, F. Wan, Q. Zhao, T. P. Yu, and J. X. Li., preprint, arXiv: 2508.16220 (2025).
64. L. X. Hu, T. P. Yu, Y. Cao, M. Chen, D. B. Zou, Y. Yin, Z. M. Sheng, and F. Q. Shao, High Power Laser Sci. Eng. **12**, e69 (2024).
65. Y. Shi, X. M. Zhang, A. Arefiev, and B. F. Shen, Sci. China Phys. Mech. Astron. **67**, 295201 (2024).
66. Y. Shi, A. Arefiev, J. X. Hao, and J. Zheng, Phys. Rev. Lett. **130**, 155101 (2023).
67. L. Y. Zhang, H. Zhang, J. Y. Wang, X. Y. Li, and T. P. Yu, High Power Laser Sci. Eng. **13**, e76 (2025).
68. N. Jain, T. M. Antonsen, and J. P. Palastro, Phys. Rev. Lett. **115**, 195001 (2015).
69. G. B. Zhang, M. Chen, J. Luo, M. Zeng, T. Yuan, J. Y. Yu, Y. Y. Ma, T. P. Yu, L. L. Yu, S. M. Weng, and Z. M. Sheng, J. Appl. Phys. **119**, 103101 (2016).
70. C. Thaury, E. Guillaume, S. Corde, R. Lehe, M. Le Bouteiller, K. T. Phuoc, X. Davoine, J. M. Rax, A. Rousse, and V. Malka, Phys. Rev. Lett. **111**, 135002 (2013).
71. F. Wan, C. Lv, K. Xue, Z. K. Dou, Q. Zhao, M. Ababekri, W. Q. Wei, Z. P. Li, Y. T. Zhao, and J. X. Li, Matter Radiat. Extremes **8**, 064002 (2023).
72. A. Ilderton, Phys. Rev. D **99**, 085002 (2019).
73. A. Di Piazza, M. Tamburini, S. Meuren, and C. H. Keitel, Phys. Rev. A **99**, 022125 (2019).
74. A. Di Piazza, M. Tamburini, S. Meuren, and C. H. Keitel, Phys. Rev. A **98**, 012134 (2018).
75. V. I. Ritus, Sov. Phys. JETP **30**, 052805 (1970).
76. V. I. Ritus, Ann. Phys. **69**, 555 (1972).
77. J. Koga, T. Z. Esirkepov, and S. V. Bulanov, Phys. Plasmas **12**, 093106 (2005).
78. W. H. McMaster, Rev. Mod. Phys. **33**, 8 (1961).
79. Y. F. Li, R. Shaisultanov, K. Z. Hatsagortsyan, F. Wan, C. H. Keitel, and J. X. Li, Phys. Rev. Lett. **122**, 154801 (2019).
80. I. P. Ivanov, Prog. Part. Nucl. Phys. **127**, 103987 (2022).
81. A. Sampath, X. Davoine, S. Corde, L. Gremillet, M. Gilljohann, M. Sangal, C. H. Keitel, R. Ariniello, J. Cary, H. Ekerfelt, C. Emma, F. Fiuza, H. Fujii, M. Hogan, C. Joshi, A. Knetsch, O. Kononenko, V. Lee, M. Litos, K. Marsh, Z. Nie, B. O'Shea, J. R. Peterson, P. San Miguel Claveria, D. Storey, Y.-P. Wu, X.-L. Xu, C.-J. Zhang, and M. Tamburini, Phys. Rev. Lett. **126**, 064801 (2021).
82. R. Babjak, L. Willingale, A. Arefiev, and M. Vranic, Phys. Rev. Lett. **132**, 125001 (2024).

https://doi.org/10.1017/hpl.2026.10121 Published online by Cambridge University Press

83. C. Aniculaesei, T. Ha, S. Yoffe, L. Labun, S. Milton, E. McCary, M. M. Spinks, H. J. Quevedo, O. Z. Labun, R. Sain, A. Hannasch, R. Zgadzaj, I. Pagano, J. A. Franco-Altamirano, M. L. Ringuette, E. Gaul, S. V. Luedtke, G. Tiwari, B. Ersfeld, E. Brunetti, H. Ruhl, T. Ditmire, S. Bruce, M. E. Donovan, M. C. Downer, D. A. Jaroszynski, and B. M. Hegelich, Matter Radiat. Extremes **9**, 014001 (2023).
84. C. Clarke, E. Esarey, C. Geddes, G. Hofstaetter, M. J. Hogan, S. Nagaitsev, M. Palmer, P. Piot, J. Power, C. Schroeder, D. Umstadter, N. Vafaei-Najafabadi, A. Valishev, L. Willingale, and V. Yakimenko, J. Instrum. **17**, T05009 (2022).
85. V. Yakimenko, L. Alsberg, E. Bong, G. Bouchard, C. Clarke, C. Emma, S. Green, C. Hast, M. J. Hogan, J. Seabury, *et al.*, Phys. Rev. Accel. Beams **22**, 101301 (2019).
86. V. Yakimenko, S. Meuren, F. D. Gaudio, C. Baumann, A. Fedotov, F. Fiuza, T. Grismayer, M. J. Hogan, A. Pukhov, L. O. Silva, and G. White, Phys. Rev. Lett. **122**, 190404 (2019).
87. W. Heitler, *The Quantum Theory of Radiation* (Clarendon Press, 1954).
88. T. D. Arber, K. Bennett, C. S. Brady, A. Lawrence-Douglas, M. G. Ramsay, N. J. Sircombe, P. Gillies, R. G. Evans, H. Schmitz, A. R. Bell, and C. P. Ridgers, Plasma Phys. Control. Fusion **57**, 113001 (2015).
89. M. V. Ammosov, N. B. Delone, and V. P. Krainov, Sov. Phys. JETP **64**, 1191 (1986).
90. J. H. Posthumus, M. R. Thompson, L. J. Frasinski, and K. Codling, in *Institute of Physics Conference Series* (1997), p. 298.
91. N. J. Carron, Prog. Electromagn. Res. **28**, 147 (2000).
92. W. Han, Y. F. Yang, W. Cheng, and Q. W. Zhan, Opt. Express **21**, 20692 (2013).
93. F. Wan, Y. Wang, R. T. Guo, Y. Y. Chen, R. Shaisultanov, Z. F. Xu, K. Z. Hatsagortsyan, C. H. Keitel, and J. X. Li, Phys. Rev. Res. **2**, 032049 (2020).
94. M. Eingorn, L. Fernando, B. Vlahovic, C. Ilie, B. Wojtsekhowski, G. M. Urciuoli, F. De Persio, F. Meddi, and V. Nelyubin, J. Astron. Telesc. Instrum. Syst. **4**, 011006 (2018).
95. C. Ilie, Publ. Astron. Soc. Pac. **131**, 111001 (2019).

https://doi.org/10.1017/hpl.2026.10121 Published online by Cambridge University Press